Fourier-transform spectroscopy combined with a 5-fs broadband pulse for multispectral nonlinear microscopy

Keisuke Isobe,[1,*] Akira Suda,[1] Masahiro Tanaka,[2] Fumihiko Kannari,[2] Hiroyuki Kawano,[3] Hideaki Mizuno,[3] Atsushi Miyawaki,[3] and Katsumi Midorikawa[1]

[1]*Laser Technology Laboratory, RIKEN 2-1 Hirosawa, Wako, Saitama 351-0198, Japan*

[2]*Department of Electronics and Electrical Engineering, Keio University, 3-14-1 Hiyoshi, Kohoku-ku, Yokohama 223-8522, Japan*

[3]*Laboratory for Cell Function Dynamics, Brain Science Institute, RIKEN 2-1 Hirosawa, Wako, Saitama 351-0198, Japan*

(Received 21 January 2008; published 23 June 2008)

We propose a technique for distinguishing the origin of a four-wave mixing (FWM) signal. This technique is based on nonlinear Fourier-transform spectroscopy (FTS) combined with the use of a broadband pulse. We theoretically analyze FWM-FTS and show that the response function in FWM is obtained from the FWM power spectrum calculated by the Fourier transform of an interferometric autocorrelation signal. When a broadband pulse is employed as an excitation light source, the FWM power spectrum shows not only Raman resonance but also two-photon electronic resonance. By comparing the FWM power spectrum of a resonant sample with that of a nonresonant reference sample, the origin of FWM is identified. By employing theoretical analysis, we experimentally demonstrate FWM-FTS using a 5-fs broadband pulse. By combining the use of a 5-fs pulse with nonlinear FTS based on two-photon excited fluorescence, we also successfully measured a two-photon excitation spectrum with a bandwidth of 300 nm.

DOI: 10.1103/PhysRevA.77.063832 PACS number(s): 42.62.Fi, 42.65.−k, 42.65.Dr, 87.64.K−

I. INTRODUCTION

Nonlinear optical microscopy [1–10] has become a powerful tool for investigating biological phenomena because of its advantages over conventional optical microscopy. The advantages are made possible by the localization of interaction volume in three-dimensional space. They include three-dimensional imaging capability, the confinement of photoinduced damage in only the focal volume, and the ability to obtain localized spectroscopic information. Note that spectroscopic information can be used to identify molecules.

There are three techniques for obtaining spectroscopic information by nonlinear optical spectroscopy. One technique is the swept-source method. In the swept-source method, the central wavelength of a narrowband laser pulse can be tuned to various excitation wavelengths and the wavelength dependence of signal intensity is then obtained sequentially [8,11]. The wavelength tuning takes some time. Another technique is the multiplex method using a combination of a broadband light source and a narrowband light source [12–15]. By exciting molecules to various excited states simultaneously, the wavelength dependence of signal intensity is measured without tuning the wavelength. In both methods, there is a trade-off between spectral resolution and the excitation efficiency of nonlinear optical processes. The reason for this is as follows. Spectral resolution depends on the spectral width of the excitation light. Pulse duration is inversely proportional to spectral width, and excitation efficiency increases with shortening pulse duration of the excitation light. Therefore, the excitation efficiency is low if the spectral resolution is high.

The last technique is the nonlinear Fourier-transform method [16,17]. Fourier-transform spectroscopy (FTS) can be applied to Raman-resonant four-wave mixing (FWM) [16,17], two-photon excited fluorescence (TPEF) [18], and sum-frequency generation [19,20]. These techniques can solve the trade-off between spectral resolution and excitation efficiency. The spectrum is obtained by the Fourier transformation of an interferometric autocorrelation (IAC) signal. Thus, the spectral resolution is determined not by the spectral width of the excitation light source, but by the inverse of maximum delay time between excitation pulses. Therefore, a high spectral resolution can be achieved even though a single broadband pulse laser that produces sub-10-fs pulses is used. Recently, broadband pulses with a pulse duration of 20 fs have been used in nonlinear FTS [21,22]. Such broadband pulses enable simultaneous measurement over a wide range of spectra and efficient molecular excitations. In the case of the use of broadband pulses, it is advantageous that the pulses are tightly focused with a high numerical-aperture (NA) objective lens because the phase matching condition in a coherent nonlinear process is markedly relaxed owing to the wide cone of wave vectors and the small interaction length. With tight focusing, excitation efficiency is also enhanced by increasing intensity. However, it is difficult to generate a tightly focused pulse whose pulse duration is shorter than 10 fs because lens chromaticity and spherical aberration lead not only to spatial distortion but also to an unfavorable pulse broadening at larger apertures [23], and the dispersion of a high NA objective becomes serious. Only two groups have reported sub-10-fs pulses at the focal point of an objective with a high NA [23,24]. In spite of some studies of Raman-resonant FWM-FTS, FWM-FTS based on two-photon electronic resonance has not been reported. One possible reason is that it is hard to generate a tightly focused pulse with a pulse duration as short as 5 fs, which is required for observing the effects of electronic resonance. Another reason is that an FWM-IAC signal due to two-photon electronic resonance contribution has not been analyzed and it

*kisobe@riken.jp

has not been shown how to acquire an electronic spectrum from an FWM-IAC signal. Moreover, it has been difficult to distinguish the origin of the FWM signal because the wavelength of the FWM signal does not depend on the contributions of Raman resonance, electronic resonance, and nonresonance.

In this paper, we propose nonlinear FTS, which can discriminate the origin of FWM. This technique is based on the use of an ultrabroadband pulse with a pulse duration of 5 fs and allows the measurement of the effects of not only Raman resonance but also two-photon electronic resonance. By taking account of the FWM-IAC signal, including the response function of a sample, we theoretically analyze FWM-FTS using an ultrabroadband pulse and show that in the FWM power spectrum there are frequency components that indicate the effects of two-photon electronic resonance and Raman resonance. By focusing on the frequency components, the origin of FWM is identified. By employing theoretical analysis, we experimentally demonstrate nonlinear FTS using a tightly focused pulse with a duration of 5 fs and measure Raman and two-photon electronic spectra in FWM. By combining the use of the 5-fs pulse with nonlinear FTS based on two-photon excited fluorescence, we also measure a two-photon excitation spectrum with a bandwidth of 300 nm. In Sec. II, we start with a discussion of nonlinear FTS. In Sec. III, we report on experiments on nonlinear FTS. In Sec. IV, we discuss a means of further improving our system. In Sec. V, we summarize this paper.

II. THEORY OF NONLINEAR FOURIER-TRANSFORM SPECTROSCOPY COMBINED WITH THE USE OF A SINGLE BROADBAND PULSE LASER

We first show the principle of nonlinear FTS combined with the use of a single broadband pulse laser. Nonlinear FTS is based on IAC measurement. The nth-order IAC signal $S_n(\tau)$ is given by

$$S_n(\tau) = \int_{-\infty}^{\infty} |P^{(n)}(t,\tau)|^2 dt, \tag{1}$$

where τ is the delay time between broadband pulses and $P^{(n)}(t,\tau)$ is the nonlinear polarization described by

$$P^{(n)}(t,\tau) = \int_0^{\infty} dt_1 \int_0^{\infty} dt_2 \cdots \int_0^{\infty} dt_n R^{(n)}(t-t_1, t-t_2, \ldots, t - t_n) E(t_1,\tau) E(t_2,\tau) \cdots E(t_n,\tau). \tag{2}$$

Here, $E(t,\tau)$ is the interferometric electric field and $R^{(n)}(t-t_1, t-t_2, \ldots, t-t_n)$ is the response function of a sample. To simplify our discussion, let us assume that a nonlinear process is due to a single-resonance contribution. Under a single-resonance condition, one of the real atomic or molecular levels is nearly coincident with one of the virtual levels of the indicated process. Second-harmonic generation (SHG), TPEF, and FWM processes are illustrated in Fig. 1. When the m-photon transition is nearly resonant, the time-delayed transition involving a real level can be separated from the instantaneous transition between virtual levels, and $R^{(n)}(t-t_1, t-t_2, \ldots, t-t_n)$ is described as

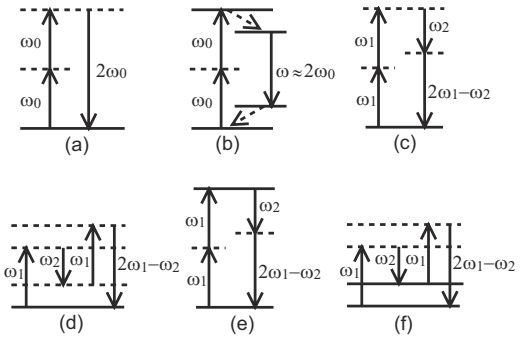

FIG. 1. Energy diagrams of SHG (a), TPEF (b), and FWM [(c)–(f)].

$$R^{(n)}(t-t_1, t-t_2, \ldots, t-t_n) = \delta(t_m - t_1) \cdots \delta(t_m - t_{m-1}) R(t-t_m) \delta(t - t_{m+1}) \cdots \delta(t-t_n). \tag{3}$$

In a nonresonance contribution, $R(t-t_m)$ is equal to $\delta(t-t_m)$ and all transitions are instantaneous. In nonlinear FTS, we calculated the power spectrum $\tilde{S}_n(\Omega)$ to obtain the spectral information $\tilde{R}(\omega)$, that is, the Fourier transform of $R(t-t_m)$. $\tilde{S}_n(\Omega)$ is obtained by the Fourier transform of the IAC signal $S_n(\tau)$ expressed by

$$\tilde{S}_n(\Omega) = \int_{-\infty}^{\infty} S_n(\tau) \exp(-i\Omega\tau) d\tau. \tag{4}$$

We analyze the IAC signal and power spectra of TPEF and FWM. We also show that the response function can be derived from the IAC signal.

A. Two-photon excited fluorescence and second-harmonic generation

We present that two-photon excitation spectra in SHG and TPEF processes shown in Figs. 1(a) and 1(b) can be obtained from the second-order IAC signal. In TPEF and SHG processes, the signal intensity is proportional to the square of incident intensity. If two-photon transition is nearly resonant, the response function is given by $R^{(2)}(t-t_1, t-t_2) = \delta(t_1 - t_2) R^{(2)}(t-t_1)$. By using this response function, the nonlinear polarizations $P^{(2)}(t,\tau)$ in TPEF and SHG are given by

$$P^{(2)}(t,\tau) = \int_{-\infty}^{\infty} R^{(2)}(t-t_1) E(t_1,\tau)^2 dt_1, \tag{5}$$

where we represent the interferometric field $E(t,\tau)$ as

$$E(t,\tau) = [A(t) + A(t-\tau)\exp(-i\omega_0\tau)]\exp(i\omega_0 t). \tag{6}$$

Here, we define the electric fields as $E(t) = A(t)\exp(i\omega_0 t)$, where $A(t)$ is a slowly varying amplitude and ω_0 is the central frequency of the electric field. The specific condition, under which the concept of envelope equations can be applicable to the single cycle regime [25], is satisfied in the following discussion. By inserting Eq. (6) into Eq. (5), we obtain

$$P^{(2)}(t,\tau) = H_1(t) + 2H_2(t,\tau)\exp(-i\omega_0\tau) + H_3(t,\tau)\exp(-i2\omega_0\tau), \quad (7)$$

where we define $H_1(t)$, $H_2(t,\tau)$, and $H_3(t,\tau)$ as

$$H_1(t) = \int R^{(2)}(t-t_1)A(t_1)^2 \exp(i2\omega_0 t_1)dt_1, \quad (8)$$

$$H_2(t,\tau) = \int R^{(2)}(t-t_1)A(t_1)A(t_1-\tau)\exp(i2\omega_0 t_1)dt_1, \quad (9)$$

$$H_3(t,\tau) = \int R^{(2)}(t-t_1)A(t_1-\tau)^2 \exp(i2\omega_0 t_1)dt_1. \quad (10)$$

Substituting Eq. (7) into Eq. (1), the second-order IAC signal $S^{(2)}(\tau)$ can be expressed as

$$\begin{aligned} S^{(2)}(\tau) = \int dt[&|H_1(t)|^2 + 4|H_2(t,\tau)|^2 + |H_3(t,\tau)|^2 \\ &+ 2\{H_1(t)H_2^*(t,\tau) + H_2(t)H_3^*(t,\tau)\}\exp(i\omega_0\tau) \\ &+ 2\{H_1^*(t)H_2(t,\tau) + H_2^*(t)H_3(t,\tau)\}\exp(-i\omega_0\tau) \\ &+ H_1(t)H_3^*(t,\tau)\exp(i2\omega_0\tau) + H_1^*(t)H_3(t,\tau) \\ &\times\exp(-i2\omega_0\tau)]. \end{aligned} \quad (11)$$

The second-order IAC signal is composed of fringe components at frequencies of around 0, ω_0, and $2\omega_0$, and the fringe contrast $S^{(2)}(0)/S^{(2)}(\infty)$ is 8. We show that the response function can be obtained from the fringe component at a frequency of around $2\omega_0$. The power spectrum at a frequency of around $2\omega_0$ is given by

$$\begin{aligned} \tilde{S}^{(2)}_{2\omega_0}(\Omega) &= \iint H_1(t)H_3^*(t,\tau)\exp(i2\omega_0\tau)dt\exp(-i\Omega\tau)d\tau \\ &= \int\int\int dtdt_1d\tau H_1(t)\exp(-i\Omega t)R^{(2)*}(t-t_1) \\ &\quad\times\exp\{[i\Omega(t-t_1)]\}A^*(t_1-\tau)^2 \\ &\quad\times\exp\{i(\Omega-2\omega_0)(t_1-\tau)\} \\ &= \tilde{R}^{(2)*}(\Omega)\tilde{A}^{(2)*}(\Omega-2\omega_0)\tilde{H}_1(\Omega) \\ &= |\tilde{R}^{(2)}(\Omega)|^2|\tilde{A}^{(2)}(\Omega-2\omega_0)|^2, \end{aligned} \quad (12)$$

where $\tilde{A}^{(2)}(\Omega)$ and $H_1(\Omega)$ are described by $\tilde{A}^{(2)}(\Omega) = \int\tilde{A}(\Omega_1)\tilde{A}(\Omega-\Omega_1)d\Omega_1$ and $\tilde{H}_1(\Omega) = R^{(2)}(\Omega)A^{(2)}(\Omega-2\omega_0)$, respectively. $|\tilde{A}^{(2)}(\Omega-2\omega_0)|^2$ is the SH power spectrum obtained from a nonresonant reference sample and is determined by the property of excitation pulses. Using a nonresonant SHG crystal such as an ultrathin β-barium borate (BBO) crystal or a two-photon diode, $|\tilde{A}^{(2)}(\Omega-2\omega_0)|^2$ can be measured. Therefore, we can obtain the response function $|\tilde{R}^{(2)}(\Omega)|^2$ by dividing the SH power spectrum of a resonant sample by that of a nonresonant reference sample. It is noted that in the theoretical derivation, there is no need to take care of a difference between dispersions of the resonant sample and the nonresonant reference sample. This is because the dispersion has a negligible effect in the broadband pulse due to the short interaction length resulting from tight focusing.

B. Four-wave mixing

In a three-photon parametric process, there are three possible resonance conditions, namely, one-photon transition, two-photon transition, and three-photon transition are nearly resonant. In the case of the one-photon resonance, the incident field experiences linear absorption and is rapidly attenuated as it propagates through the sample. Similarly, in the case of the three-photon resonance, the generated field experiences linear absorption. However, in the case of the two-photon resonance, the generated field experiences no linear absorption. Therefore, to generate signals efficiently, the two-photon resonance is used. In FWM, a photon with a frequency of $2\omega_1-\omega_2$ is generated by the interaction between the medium and photons with frequencies of ω_1 and ω_2. In two-photon resonance FWM, electronic resonance [Fig. 1(e)] and Raman resonance [Fig. 1(f)] exist. The frequency of the FWM signal does not depend on the contributions of Raman resonance and electronic resonance. To discriminate the signal under the electronic resonance from that under the Raman resonance, it has been necessary to measure the dependences of signal intensity on pump frequency $(2\omega_1)$ and frequency difference $(\omega_1-\omega_2)$. In this section, we show that the origin of the FWM signal can be distinguished by taking advantage of the FWM power spectrum obtained by nonlinear FTS.

We analyze the FWM power spectrum obtained by the Fourier transform of the third-order IAC signal by FWM under the two-photon electronic (TPE) resonance. The polarization in FWM under the TPE resonance is described by

$$P^{(\mathrm{TPE})}(t,\tau) = E_2^*(t,\tau)\int R^{(\mathrm{TPE})}(t-t_1)E_1(t_1,\tau)^2dt_1, \quad (13)$$

where $E_i(t,\tau) = [A_i(t) + A_i(t-\tau)\exp(-i\omega_i\tau)]\exp(i\omega_i t)$, $(i=1,2)$. The absolute square of $P^{(\mathrm{TPE})}(t,\tau)$ is expressed as

$$\begin{aligned} |P^{(\mathrm{TPE})}(t,\tau)|^2 = {} & B_0(t,\tau) + B_1(t,\tau)\exp(i\omega_2\tau) + B_1^*(t,\tau)\exp(-i\omega_2\tau) + B_2(t,\tau)\exp(i\omega_1\tau) + B_2^*(t,\tau)\exp(-i\omega_1\tau) \\ & + B_3(t,\tau)\exp\{i(\omega_1+\omega_2)\tau\} + B_3^*(t,\tau)\exp\{-i(\omega_1+\omega_2)\tau\} + B_4(t,\tau)\exp\{i(\omega_1-\omega_2)\tau\} \\ & + B_4^*(t,\tau)\exp\{-i(\omega_1-\omega_2)\tau\} + B_5(t,\tau)\exp(i2\omega_1\tau) + B_5^*(t,\tau)\exp(-i2\omega_1\tau) + B_6(t,\tau)\exp\{i(2\omega_1-\omega_2)\tau\} \\ & + B_6^*(t,\tau)\exp\{-i(2\omega_1-\omega_2)\tau\} + B_7(t,\tau)\exp\{i(2\omega_1+\omega_2)\tau\} + B_7^*(t,\tau)\exp\{-i(2\omega_1+\omega_2)\tau\}, \end{aligned} \quad (14)$$

where we define $B_0(t,\tau)$, $B_1(t,\tau)$, $B_2(t,\tau)$, $B_3(t,\tau)$, $B_4(t,\tau)$, $B_5(t,\tau)$, $B_6(t,\tau)$ and $B_7(t,\tau)$ as

$$B_0(t,\tau) = [|A_2(t)|^2 + |A_2(t-\tau)|^2][|F_1(t)|^2 + 4|F_2(t,\tau)|^2 + |F_3(t,\tau)|^2], \tag{15}$$

$$B_1(t,\tau) = A_2(t)A_2^*(t-\tau)[|F_1(t)|^2 + 4|F_2(t,\tau)|^2 + |F_3(t,\tau)|^2], \tag{16}$$

$$B_2(t,\tau) = 2[|A_2(t)|^2 + |A_2(t-\tau)|^2][F_1(t)F_2^*(t,\tau) + F_2(t,\tau)F_3^*(t,\tau)], \tag{17}$$

$$B_3(t,\tau) = 2A_2(t)A_2^*(t-\tau)[F_1(t)F_2^*(t,\tau) + F_2(t,\tau)F_3^*(t,\tau)], \tag{18}$$

$$B_4(t,\tau) = 2A_2^*(t)A_2(t-\tau)[F_1(t)F_2^*(t,\tau) + F_2(t,\tau)F_3^*(t,\tau)], \tag{19}$$

$$B_5(t,\tau) = [|A_2(t)|^2 + |A_2(t-\tau)|^2]F_1(t)F_3^*(t,\tau), \tag{20}$$

$$B_6(t,\tau) = A_2^*(t)A_2(t-\tau)F_1(t)F_3^*(t,\tau), \tag{21}$$

$$B_7(t,\tau) = A_2(t)A_2^*(t-\tau)F_1(t)F_3^*(t,\tau). \tag{22}$$

Here, we define $F_1(t)$, $F_2(t,\tau)$, and $F_3(t,\tau)$ as

$$F_1(t) = \int R^{(2)}(t-t_1)A_1(t_1)^2\exp(i2\omega_1 t_1)dt_1, \tag{23}$$

$$F_2(t,\tau) = \int R^{(2)}(t-t_1)A_1(t_1)A_1(t_1-\tau)\exp(i2\omega_1 t_1)dt_1, \tag{24}$$

$$F_3(t,\tau) = \int R^{(2)}(t-t_1)A_1(t_1-\tau)^2\exp(i2\omega_1 t_1)dt_1. \tag{25}$$

From Eq. (14), we find that the FWM-IAC signal under the TPE resonance includes fringe components at frequencies of around 0, ω_1, ω_2, $\omega_1-\omega_2$, $\omega_1+\omega_2$, $2\omega_1$, $2\omega_1-\omega_2$, and $2\omega_1+\omega_2$, and that the fringe contrast $S^{(\mathrm{TPE})}(0)/S^{(\mathrm{TPE})}(\infty)$ is 32. We focus on the fringe component at a frequency of around $2\omega_1$. The FWM power spectrum at a frequency of around $2\omega_1$ is given by

$$S_{2\omega_1}^{(\mathrm{TPE})}(\Omega) = \tilde{R}^{(\mathrm{TPE})*}(\Omega)\tilde{A}_{11}^{(2)*}(\Omega-2\omega_1)\int \tilde{A}_{22}^{(2\#)}(\Omega-\Omega_1) \times \tilde{R}^{(\mathrm{TPE})}(\Omega_1)\tilde{A}_{11}^{(2)}(\Omega_1-2\omega_1)d\Omega_1 + \tilde{R}^{(\mathrm{TPE})}(\Omega)\tilde{A}_{11}^{(2)}(\Omega-2\omega_1)\left[\int \tilde{A}_{22}^{(2\#)}(\Omega-\Omega_1) \times \tilde{R}^{(\mathrm{TPE})}(\Omega_1)\tilde{A}_{11}^{(2)}(\Omega_1-2\omega_1)d\Omega_1\right]^*, \tag{26}$$

where $\tilde{A}_{ij}^{(2\#)}(\omega) = \int \tilde{A}_i(\Omega_1)\tilde{A}_j^*(\Omega_1-\omega)d\Omega_1$ and $\tilde{A}_{ij}^{(2)}(\omega) = \int \tilde{A}_i(\Omega_1)\tilde{A}_j(\omega-\Omega_1)d\Omega_1$. In the case of the samples whose spectral bandwidth of absorption is narrow such as an atomic vapor and fluorophores at extremely low temperatures, we can assume that $\tilde{R}^{(\mathrm{TPE})}$ is $\delta(\Omega-\Omega_0)$. Then we obtain

$$S_{2\omega_1}^{(\mathrm{TPE})}(\Omega) \approx \delta(\Omega-\Omega_0)\tilde{A}_{22}^{(2\#)}(\Omega-\Omega_0)|\tilde{A}_{11}^{(2)}(\Omega_0-2\omega_1)|^2 + \delta(\Omega-\Omega_0)\tilde{A}_{22}^{(2\#)*}(\Omega-\Omega_0)|\tilde{A}_{11}^{(2)}(\Omega_0-2\omega_1)|^2. \tag{27}$$

In the FWM power spectrum at a frequency of around $2\omega_1$, the only resonant frequency component remains. Thus, the Fourier spectrum of the response function can be obtained.

On the other hand, if the spectral bandwidth of $\tilde{R}^{(\mathrm{TPE})}$ is broader than that of $\tilde{A}_{11}^{(2)}(\Omega-2\omega_1)$, we can regard $\int \tilde{A}_{22}^{(2\#)}(\Omega-\Omega_1)\tilde{R}^{(\mathrm{TPE})}(\Omega_1)\tilde{A}_{11}^{(2)}(\Omega_1-2\omega_1)d\Omega_1$ as $\int \tilde{A}_{22}^{(2\#)}(\Omega-\Omega_1)\tilde{A}_{11}^{(2)}(\Omega_1-2\omega_1)d\Omega_1$. When this approximation is made, Eq. (26) becomes

$$S_{2\omega_1}^{(\mathrm{TPE})}(\Omega) \approx \tilde{R}^{(\mathrm{TPE})*}(\Omega)\tilde{A}_{11}^{(2)*}(\Omega-2\omega_1)\int \tilde{A}_{22}^{(2\#)}(\Omega-\Omega_1)\tilde{A}_{11}^{(2)} \times(\Omega_1-2\omega_1)d\Omega_1 + \tilde{R}^{(\mathrm{TPE})}(\Omega)\tilde{A}_{11}^{(2)}(\Omega-2\omega_1) \times\left[\int \tilde{A}_{22}^{(2\#)}(\Omega-\Omega_1)\tilde{A}_{11}^{(2)}(\Omega_1-2\omega_1)d\Omega_1\right]^*. \tag{28}$$

$\tilde{A}_{11}^{(2)}(\Omega-2\omega_1)[\int \tilde{A}_{22}^{(2\#)}(\Omega-\Omega_1)\tilde{A}_{11}^{(2)}(\Omega_1-2\omega_1)d\Omega_1]^*$ can be derived from the IAC signal by FWM in a nonresonant sample. Therefore, we can obtain the response function of a resonant sample by measuring IAC signals by FWM from the two-photon resonant sample and nonresonant reference sample. However, it is required that the bandwidth of $\tilde{A}_{11}^{(2)}(\Omega-2\omega_1)$ is broad enough to acquire the response function with the wavelength dependence.

We also consider the FWM power spectrum obtained by the Fourier transform of the IAC signal by FWM under the Raman resonance. The polarization in FWM under the Raman resonance is described by

$$P^{(\mathrm{Raman})}(t,\tau) = E_1(t,\tau)\int R^{(\mathrm{Raman})}(t-t_1)E_1(t_1,\tau)E_2^*(t_1,\tau)dt_1. \tag{29}$$

We obtain the third-order FWM-IAC signal under the Raman resonance, as shown in the Appendix. The FWM-IAC signal under the Raman resonance is also composed of the fringe components at frequencies of around 0, ω_1, ω_2, $\omega_1-\omega_2$, $\omega_1+\omega_2$, $2\omega_1$, $2\omega_1-\omega_2$, and $2\omega_1+\omega_2$. The fringe component at a frequency of around $\omega_1-\omega_2$ is given by

$$S_{\omega_1-\omega_2}^{(\mathrm{Raman})}(\tau) = \int dt\{[|A_1(t)|^2 + |A_1(t-\tau)|^2]G_1(t)G_2^*(t,\tau) + A_1(t)A_1^*(t-\tau)[G_1(t)G_4^*(t,\tau) + G_2^*(t,\tau)G_3(t,\tau)]\}\exp\{i(\omega_1-\omega_2)\tau\}, \tag{30}$$

where $G_1(t)$, $G_2(t,\tau)$, $G_3(t,\tau)$, and $G_4(t,\tau)$ are expressed as

$$G_1(t) = \int R^{(\mathrm{Raman})}(t-t_1)A_1(t_1)A_2^*(t_1)\exp\{i(\omega_1-\omega_2)t_1\}dt_1, \tag{31}$$

$$G_2(t,\tau) = \int R^{(\mathrm{Raman})}(t-t_1)A_1(t_1-\tau)A_2^*(t_1-\tau) \times\exp\{i(\omega_1-\omega_2)t_1\}dt_1, \tag{32}$$

$$G_3(t,\tau) = \int R^{(\mathrm{Raman})}(t-t_1)A_1(t_1-\tau)A_2^*(t_1) \times\exp\{i(\omega_1-\omega_2)t_1\}dt_1, \tag{33}$$

$$G_4(t,\tau) = \int R^{(\mathrm{Raman})}(t-t_1)A_1(t_1)A_2^*(t_1-\tau) \times\exp\{i(\omega_1-\omega_2)t_1\}dt_1. \tag{34}$$

The FWM power spectrum at a frequency of around $\omega_1-\omega_2$ is expressed by

$$\begin{aligned}\tilde{S}^{(\mathrm{Raman})}_{(\omega_1-\omega_2)}(\Omega) &= \tilde{R}^{(\mathrm{Raman})}(\Omega)\tilde{A}^{(2\#)}_{12}(\Omega-\omega_1+\omega_2)\left[\int \tilde{A}^{(2\#)}_{11}(\Omega-\Omega_1)\tilde{R}^{(\mathrm{Raman})}(\Omega_1)\tilde{A}^{(2\#)}_{12}(\Omega_1-\omega_1+\omega_2)d\Omega_1\right]^* \\ &+ \tilde{R}^{(\mathrm{Raman})*}(\Omega)\tilde{A}^{(2\#)*}_{12}(\Omega-\omega_1+\omega_2)\left[\int \tilde{A}^{(2\#)}_{11}(\Omega-\Omega_1)\tilde{R}^{(\mathrm{Raman})}(\Omega_1)\tilde{A}^{(2\#)}_{12}(\Omega_1-\omega_1+\omega_2)d\Omega_1\right] \\ &+ \int d\Omega_1\tilde{R}^{(\mathrm{Raman})*}(\Omega_1)A_1^*(\Omega_1)\tilde{A}_1^*(\Omega_1-\Omega)\tilde{A}_2(\Omega_1-\Omega+\omega_1-\omega_2)\int \tilde{A}_1(\Omega_2)\tilde{G}_1(\Omega_1-\Omega_2)d\Omega_2 \\ &+ \int d\Omega_1\tilde{R}^{(\mathrm{Raman})}(\Omega_1)A_1(\Omega_1)\tilde{A}_1(\Omega_1-\Omega)\tilde{A}_2^*(\Omega_1-\Omega+\omega_1-\omega_2)\int \tilde{A}_1^*(\Omega_2)\tilde{G}_1^*(\Omega_1-\Omega_2)d\Omega_2,\end{aligned} \tag{35}$$

where $\tilde{G}_1(\Omega)$ is given by $\tilde{G}_1(\Omega)=\tilde{R}^{(\mathrm{Raman})}(\Omega)\tilde{A}^{(2\#)}_{12}(\Omega-\omega_1+\omega_2)$. If the delay time τ is longer than the pulse duration but is shorter than the Raman coherence lifetime, $G_1(t)$ and $G_2(t,\tau)$ are not equal to zero, whereas $G_3(t,\tau)$, $G_4(t,\tau)$, and $A_1(t)A_1^*(t-\tau)$ are equal to zero. Then, we obtain

$$\begin{aligned}S^{(\mathrm{Raman}\#)}(\tau) = \int dt[&|A_1(t)|^2|G_1(t)|^2 + |A_1(t-\tau)|^2|G_2(t,\tau)|^2 \\ &+ [|A_1(t)|^2+|A_1(t-\tau)|^2]G_1(t)G_2^*(t,\tau)\exp\{i(\omega_1-\omega_2)\tau\} + [|A_1(t)|^2+|A_1(t-\tau)|^2]G_1^*(t)G_2(t,\tau) \\ &\times\exp\{-i(\omega_1-\omega_2)\tau\}].\end{aligned} \tag{36}$$

Equation (36) indicates that when no Raman coherence is induced, no FWM signal is generated by the interaction between two pulses that are not temporally overlapped. Even though the nonresonance FWM signal or electronic resonance FWM signal are mixed with the Raman resonance FWM signal, the FWM-IAC signal shown in Eq. (36) can be obtained in a delay time longer than the pulse duration. From Eq. (36), the FWM-IAC signal under the Raman resonance condition is composed of only fringe components at frequencies of around 0 and $\omega_1-\omega_2$. The FWM power spectrum at a frequency of around $\omega_1-\omega_2$ is obtained by

$$\begin{aligned}\tilde{S}^{(\mathrm{Raman}\#)}_{(\omega_1-\omega_2)}(\Omega) &= \tilde{R}^{(\mathrm{Raman})}(\Omega)\tilde{A}^{(2\#)}_{12}(\Omega-\omega_1+\omega_2)\left[\int \tilde{A}^{(2\#)}_{11}(\Omega-\Omega_1)\tilde{R}^{(\mathrm{Raman})}(\Omega_1)\tilde{A}^{(2\#)}_{12}(\Omega_1-\omega_1+\omega_2)d\Omega_1\right]^* \\ &+ \tilde{R}^{(\mathrm{Raman})*}(\Omega)\tilde{A}^{(2\#)*}_{12}(\Omega-\omega_1+\omega_2)\left[\int \tilde{A}^{(2\#)}_{11}(\Omega-\Omega_1)\tilde{R}^{(\mathrm{Raman})}(\Omega_1)\tilde{A}^{(2\#)}_{12}(\Omega_1-\omega_1+\omega_2)d\Omega_1\right].\end{aligned} \tag{37}$$

Since the Raman bandwidth is typically on the order of 10 cm^{-1} [26], the bandwidth of $\tilde{A}^{(2\#)}_{12}(\Omega)$ in a sub-10-fs pulse is much broader than the Raman bandwidth. Therefore, we can regard $\tilde{R}^{(\mathrm{Raman})}(\Omega)$ as $\delta(\Omega-\Omega_0)$ and simplify Eq. (37) to

$$\begin{aligned}\tilde{S}^{(\mathrm{Raman}\#)}_{(\omega_1-\omega_2)}(\Omega) \approx{}& \delta(\Omega-\Omega_0)\tilde{A}^{(2\#)}_{11}(\Omega-\Omega_0)|\tilde{A}^{(2\#)}_{12}(\Omega_0-\omega_1+\omega_2)|^2 \\ &+ \delta(\Omega-\Omega_0)\tilde{A}^{(2\#)*}_{11}(\Omega-\Omega_0)|\tilde{A}^{(2\#)}_{12}(\Omega_0-\omega_1+\omega_2)|^2.\end{aligned} \tag{38}$$

Equation (38) indicates the Fourier spectrum of the response function. By measuring the FWM-IAC signal in a delay time range longer than the pulse duration but shorter than the Raman coherence time, we can obtain the response function of a Raman resonance sample.

Note that the origin of the FWM signal can be discriminated by focusing on the FWM power spectrum at frequen-

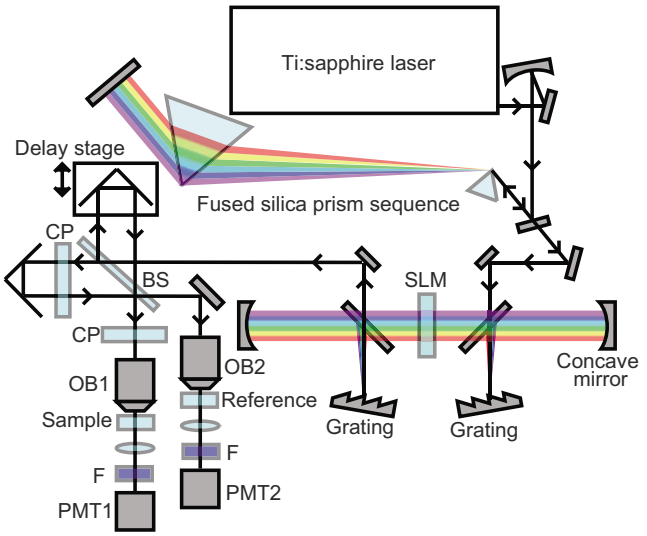

FIG. 2. (Color online) Experimental setup for nonlinear Fourier-transform spectroscopy. BS: beam splitter. OB: objective lens. CP: compensation plate. PMT: photomultiplier tube.

cies of around $2\omega_1$ or $\omega_1-\omega_2$. In the case of TPE resonance, if the resonant bandwidth is narrow, Eq. (27) without using the nonresonant reference sample can be used for obtaining the response function. If not, we must use Eq. (28) together with the signal from the nonresonant reference sample. For the Raman resonance, if the delay time is longer than the pulse duration and is shorter than the Raman coherence time, Eq. (38) without employing the nonresonant reference sample, can be applied. If not, the nonresonant reference sample is needed and Eq. (35) is used.

III. EXPERIMENTAL

A. Experimental setup

A schematic of the experimental setup is shown in Fig. 2. As a broadband light source, we used a Ti:sapphire laser (nanolayers, Venteon) operating at a repetition rate of 80 MHz. The laser spectrum ranged from 660 to 1100 nm, as shown in Fig. 3. To compensate for the dispersion of optical components before the focal point of microscope objectives (OB1 and OB2), a laser pulse was passed through a fused silica prism sequence and a grating-pair-formed pulse shaper with a liquid-crystal spatial light modulator (SLM) (Cambridge Research & Instrumentation, Inc., LC-SLM-128)

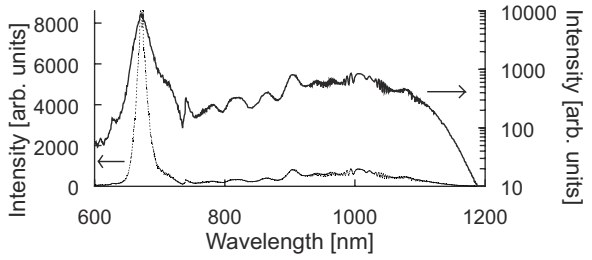

FIG. 3. Spectrum of a broadband pulse generated from a Ti:sapphire laser.

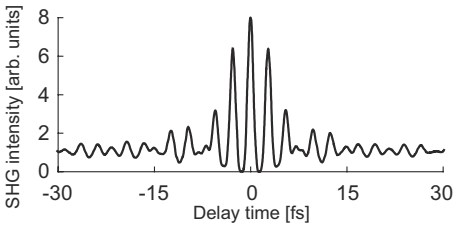

FIG. 4. SHG-IAC signal at the focal point of an objective lens.

placed at a Fourier plane. At the SLM, the spectral bandwidth was limited to around 340 nm to improve the spectral resolution of spectral phase modulation. A prechirped laser pulse was sent into a Michelson interferometer. One half of the output was focused into a resonant sample and the other half into a nonresonant reference sample by microscope objectives (OBs) (Olympus Corporation, UPLSAPO40×, NA 0.9) whose chromatic and spherical aberrations were optimized for the spectral region from the visible region to the near-infrared region. Each resultant signal was detected with a photomultiplier tube (PMT) (Hamamatsu Photonics, R7400U-6) after excitation light was eliminated by an excitation-light cut filter (Showa Optronics Co., Ltd., broadband dichroic filter for a Ti:sapphire laser). IAC signals were obtained by scanning a piezoelectric transducer stage with a step size of 5 nm, which corresponds to a delay time of 33 fs. The maximum delay time was 533 fs.

B. Generation of tightly focused pulse with a duration of 5 fs

We generated a Fourier-transform-limited (FTL) pulse at the focal point of the objectives with the SLM phase mask obtained by simulated annealing (SA). In SA, the pulse from one arm of the interferometer was focused onto a 10-μm-thick BBO crystal, and an SLM phase mask for maximizing the resultant SHG was searched. The optimized pulses were measured by the SHG-IAC method. Figure 4 shows the obtained IAC signal. With a deconvolution factor of 1.48, we estimated the pulse duration to be 5.3 fs. The deconvolution factor was obtained from the relationship between the theoretical FTL pulse with a duration of 5.1 fs and its IAC signal with a full width at half maximum of 7.6 fs. By correcting the spherical and chromatic aberrations of the microscope objective, we could generate a tightly focused pulse with a duration of 5.3 fs.

C. Measurement of excitation spectra in two-photon excited fluorescence

To confirm the measurable spectral bandwidth in TPEF, we measured second-order IAC signals from the fluorescent proteins SeBFP and Venus. The concentration of the fluorescent protein solutions was 30 mg/c^3. A 10-μm-thick BBO crystal was used as a reference sample. In this experiment, the excitation spectrum was limited to the region from 700 to 1040 nm by the SLM and the power at the focal point of each arm in the interferometer was 1 mW. Figure 5(a) shows the SH power spectra obtained by the Fourier transform of

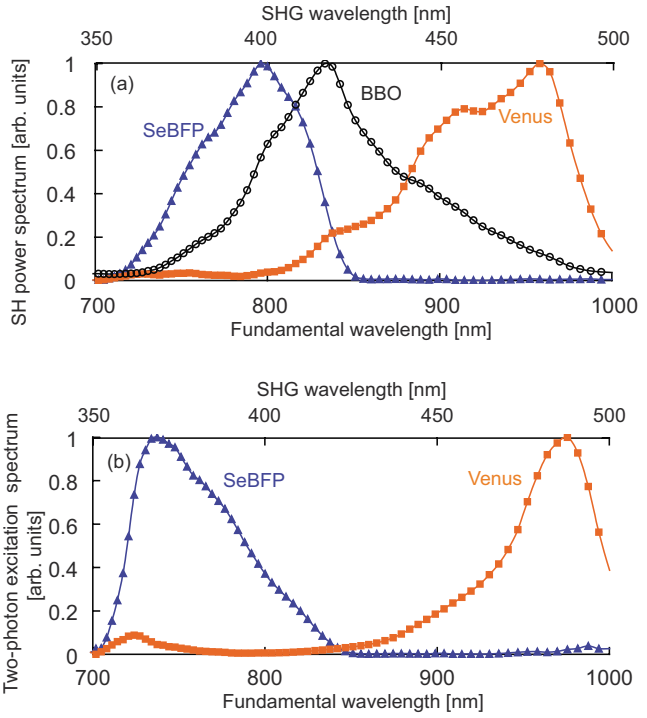

FIG. 5. (Color online) (a) SH power spectra obtained by the Fourier transform of a second-order IAC signal from a BBO crystal (black circle line), SeBFP (blue triangle line), and Venus (orange square line). (b) Two-photon excitation spectra of SeBFP (blue triangle line) and Venus (orange square line).

the second-order IAC signals. The black circle, blue triangle, and orange square lines indicate the SH power spectra of the BBO crystal, SeBFP, and Venus, respectively. Two-photon excitation spectra were obtained by dividing the SH power spectra of the fluorescent proteins by that of the BBO crystal. The two-photon excitation spectra obtained are shown in Fig. 5(b). We found that two-photon excitation spectra are similar to one-photon excitation spectra [27]. The measurable spectral width in this experiment was four times as broad as that in Ref. [21]. Note that the measurable spectral bandwidth is 300 nm, which covers the wavelength tuning range of a narrowband Ti:sapphire laser.

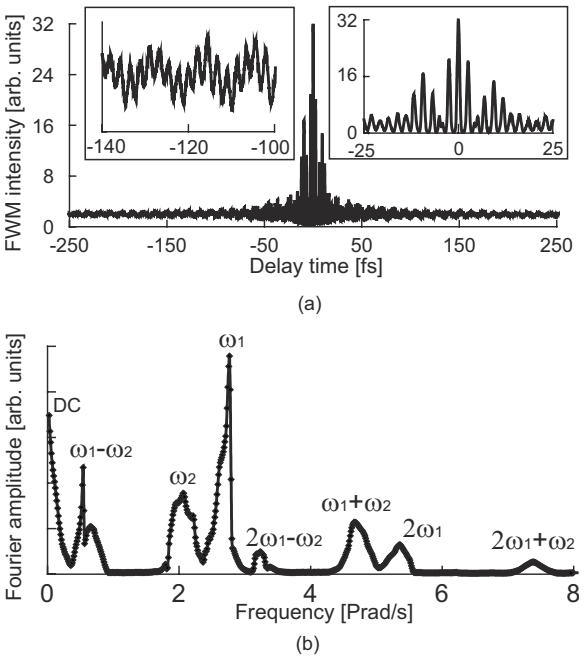

FIG. 6. (a) FWM-IAC signal of acetone. (b) FWM power spectrum obtained by the Fourier transform of the FWM-IAC signal shown in (a).

D. Measurement of Raman and two-photon electronic spectra in four-wave mixing

To demonstrate identification of the origin of the FWM signal, we measured the FWM-IAC signals that were due to the Raman or two-photon electronic contribution. We limited the spectral bandwidth at the SLM so that the excitation spectrum ranged from 660 to 1000 nm. Taking advantage of the broadband spectrum, we utilized the intrapulse FWM effect induced by electric field components with frequencies of ω_1 and ω_2 in a single broadband pulse. The wavelength of the FWM signal was around 580 nm. The short-wavelength components around 700 nm acted as two pump pulses with a frequency of ω_1, while the long-wavelength components around 900 nm served as a pulse with a frequency of ω_2.

To confirm the Raman resonance effect in the FWM-IAC measurement, we used an organic solvent as the sample with Raman resonance. Figure 6(a) shows the FWM-IAC signal obtained from acetone. The Fourier transform of the FWM-IAC signal is shown in Fig. 6(b). We found that in the Fourier spectrum, there were frequency components of 0,

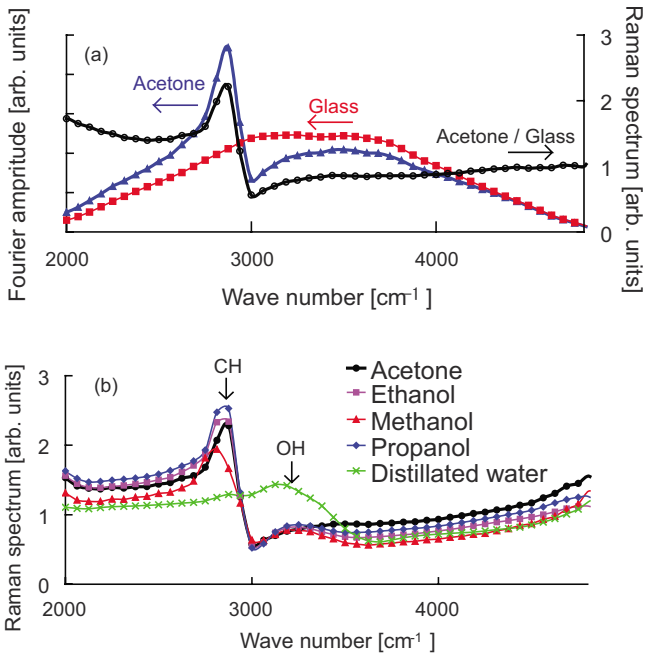

FIG. 7. (Color online) FWM power spectra at a frequency of around $\omega_1-\omega_2$ and Raman spectra. (a) FWM power spectra of acetone (blue triangle line) and cover glass (red square line), and Raman spectrum of acetone (black circle line). (b) Raman spectra of acetone (black circle line), propanol (blue diamond line), ethanol (pink square line), methanol (red triangle line), and distilled water (green cross line).

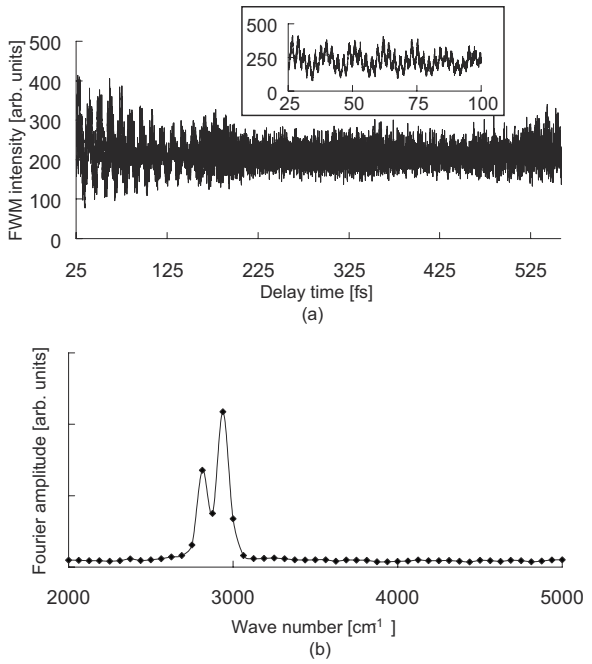

FIG. 8. (a) FWM-IAC signal with a delay time longer than pulse duration but shorter than Raman coherence time. (b) FWM power spectrum obtained by the Fourier transform of the FWM-IAC signal shown in (a).

$\omega_1-\omega_2$, ω_1, ω_2, $2\omega_1-\omega_2$, $\omega_1+\omega_2$, $2\omega_1$, and $2\omega_1+\omega_2$. We focused only on the frequency component of $\omega_1-\omega_2$. The blue triangle line in Fig. 7(a) shows a magnified view of the frequency component at around $\omega_1-\omega_2$ in Fig. 6(a). To compare the FWM power spectrum of acetone with that of the nonresonant sample, we measured the FWM-IAC signal from a cover glass. The FWM power spectrum of a cover glass is shown by the red square line in Fig. 7(a). We found that the frequency components at a wave number of around 2937 cm^{-1} were enhanced. This wave number is identified by the CH stretching vibration. The black line in Fig. 7(a) indicates the FWM Raman spectrum obtained by dividing the FWM power spectrum of acetone by that of the cover glass. This FWM Raman spectrum included the nonresonant contribution that is uniform against frequency. We measured the FWM Raman spectra of ethanol, propanol, methanol, and distilled water. The Raman resonance effect in Fig. 7(b) is due to the CH stretching vibration and the OH stretching vibration in the range of 3100–3600 cm^{-1}. It must be emphasized that the Raman spectrum with a bandwidth of 3000 cm^{-1} can be measured simultaneously.

To remove the effect of the instantaneous response due to the electronic contribution, we measured the FWM-IAC signal in a delay time range longer than the pulse duration. The sample was ethanol. The FWM-IAC signal and its Fourier transform are shown in Figs. 8(a) and 8(b). We found that this power spectrum includes no electronic contribution. Note that a pure Raman spectrum can be obtained without the use of a nonresonant reference sample. However, the Raman resonance effect in Fig. 8(b) is due to only the CH stretching vibration. We could not find the contribution of the OH stretching vibration in the range of 3100–3600 cm^{-1}.

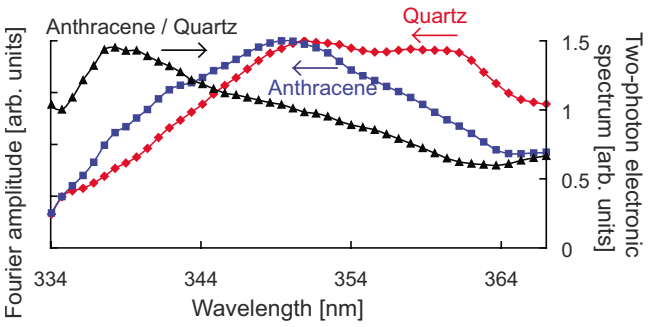

FIG. 9. (Color online) (a) FWM power spectra at a frequency of around $2\omega_1$ and a two-photon electronic spectrum. FWM power spectra of anthracene (blue square line) and quartz (red diamond line), and a two-photon electronic spectrum of anthracene (black triangle line).

This result indicates that the resonance bandwidth of the OH vibration is broad enough to be the Raman coherence time shorter than the delay time region.

Next, we measured the FWM-IAC signal due to the two-photon electronic resonance contribution. The sample used was an anthracene powder whose resonant frequency was around 350 nm. Under the TPE resonance condition, a TPEF was also generated from the anthracene powder. A bandpass filter (Semrock, Inc., FF01-593/40) was used for eliminating the TPEF. We used quartz as the nonresonant reference sample. To confirm the TPE resonance effect, we focused on the frequency components at a frequency of around $2\omega_1$. This frequency corresponded to a wavelength of 350 nm. The FWM power spectra of the anthracene powder and quartz are shown by the blue square and red diamond lines in Fig. 9, respectively. The black triangle line in Fig. 9 indicates the TPE spectrum obtained by dividing the power spectrum of the anthracene powder by that of quartz. The wavelength dependence under the TPE resonance appeared clearly. By using a 5-fs broadband pulse, we could observe the two-photon electronic resonance effect. Taking advantage of the power spectrum obtained by the Fourier transform of the FWM-IAC signal, we could identify the origin of the FWM signal. Nonlinear FTS is found to be a remarkably effective tool for discriminating the origin of the FWM signal.

IV. DISCUSSION

As shown in the above experiment, our Fourier-transform spectroscopy gives Raman spectra that range from 2000 to 5000 cm^{-1}. Although the shortest wavelength of the pump light in this experiment was 660 nm, the longest wavelength of the measured FWM signal was limited to 600 nm by the excitation light cut filter. This leads to the suppression of the measurable bandwidth of the Raman spectrum because the IAC signal composed of the FWM signal with a wavelength range from 600 to 660 nm produces a Raman spectrum in a wave number region shorter than 2000 cm^{-1}. We can predict that the measurable bandwidth of Raman spectrum can be improved to 5000 cm^{-1} using an excitation light cut filter with a cutoff wavelength of 650 nm. This bandwidth covers the Raman fingerprint region. By using this filter, the mea-

surable bandwidth of TPE spectrum can also be increased. Another way to improve our system is to change the spectral bandwidth at the SLM. If a full laser spectrum is used and the number of pixels in the SLM is increased, we can compensate for the dispersion in the full laser spectrum and improve the spectral bandwidth of the frequency components that contribute to the intrapulse FWM signal. Thus, the measurable bandwidth of Raman and TPE spectra can be increased.

The Raman spectrum with the electronic contribution was different from that without the electronic contribution. The Raman spectrum with the electronic contribution is the absolute value of the sum of the instantaneous electronic and the delayed Raman responses because of the interference of FWM signals generated by the instantaneous electronic and the delayed Raman responses. Since the instantaneous electronic response is only a real part that is independent of frequency, the real and imaginary parts in the entire response function are the sum of the large real part in the instantaneous electronic response and the real part in the delayed Raman response, and the imaginary part in the delayed Raman response, respectively. Thus, the real part is the dominant contribution in the absolute value of the entire response function and the absolute value of the entire response function is similar to the real part in the delayed Raman response. Without the instantaneous electronic response, the absolute value of the entire response function is determined only by the absolute value of the delayed Raman response.Therefore, it would be advantageous that the IAC signal is measured in a delay time longer than the pulse duration. However, in the case of the measurement of vibrational modes with a short Raman coherence time such as the OH stretching vibration, it is necessary to obtain an IAC signal in a delay time region including the electronic contribution. By shortening the pulse duration, the vibrational modes with a short Raman coherence time can be measured in the delay time region longer than the pulse duration.

We achieved the acquirement of a two-photon excitation spectrum that ranged from 700 to 1040 nm. The short wavelength tail of the measurable two-photon excitation spectrum tends to be overlapped with the long wavelength tail of the one-photon excitation spectrum of visible fluorophores. In such a case, it is difficult that the swept-source method is applied to obtaining the TPE spectrum. This is because both TPEF and one-photon excited fluorescence (OPEF) signals are simultaneouly generated at the same laser wavelength. This problem can be solved by nonlinear FTS. In nonlinear FTS, the fringe components at $2\omega_0$ are composed of only TPEF signals. Therefore, TPEF signals can be easily separated from OPEF signals. This advantage is also useful for spectroscopy based on higher-order nonlinear processes.

Taking advantage of FTS, we can combine FWM microscopy based on TPE resonance with that based on Raman resonance. By using both Raman and TPE spectra, we expect that the capability to identify molecules will be improved dramatically.

V. CONCLUSION

In summary, we have demonstrated nonlinear FTS with a 5-fs broadband pulse laser. We discussed the method for measuring the response function in TPEF, and FWM under the Raman resonance and TPE resonance. From our analysis, we found that the response function could be obtained by dividing the power spectrum of the resonant sample by that of the nonresonant sample. Under specific conditions, the power spectrum of the resonant sample indicates the response function and that of the nonresonant sample is not required. In the case of TPE resonance, the condition is satisfied with the narrow resonant bandwidth. In the case of Raman resonance, the condition demands the measurement in the delay time region longer than the pulse duration and shorter than the Raman coherence time. Moreover, it is required that the pulse duration is shorter than the Raman coherence time. The measurable bandwidth in nonlinear FTS increases with shortening the pulse duration. In the experiment, we generated the ultrabroadband pulse with a pulse duration of 5 fs and the ultrabroadband pulse was applied to nonlinear FTS. Two-photon excitation spectra were experimentally obtained by nonlinear FTS. The measurable bandwidth of the two-photon excitation spectra was 300 nm, which covered the wavelength tuning range of a narrowband Ti:sapphire laser. Furthermore, we demonstrated that the origin of the FWM signal could be identified by taking advantage of the power spectra obtained by the Fourier transform of the FWM-IAC signal. In the FWM power spectrum, the Raman and TPE resonance effects appeared at frequency components at frequencies of around $\omega_1-\omega_2$ and $2\omega_1$, respectively. The Raman spectrum at a bandwidth of 3000 cm^{-1} was simultaneously measured. By employing the 5-fs pulse, we succeeded in the observation of the effect of TPE resonance with FWM-FTS for the first time. Note that nonlinear FTS combined with the use of a broadband pulse is quite effective for discriminating the origin of a nonlinear signal.

ACKNOWLEDGMENTS

This research was supported by the Special Postdoctoral Researchers Program of RIKEN. This work was partly supported by a Grant-in-Aid for Scientific Research (No. 18656023) from the Ministry of Education, Culture, Sports, Science and Technology, Japan.

APPENDIX: DERIVATION OF EQUATION

1. Derivation of Eq. (26)

To derive Eq. (26), we calculate the Fourier transform of the fringe component $B_5(t,\tau)$ at a frequency of around $2\omega_1$ in the FWM-IAC signal under the TPE resonance. The Fourier transform of $B_5(t,\tau)$ is described by

$$\mathcal{T}_F[B_5(t,\tau)] = \int dt|A_2(t)|^2 F_1(t)\mathcal{T}_F[F_3^*(t,\tau)\exp(i2\omega_1\tau)] + \int dt F_1(t)\mathcal{T}_F[|A_2(t-\tau)|^2 F_3^*(t,\tau)\exp(i2\omega_1\tau)], \tag{A1}$$

where $\mathcal{T}_F[f(\tau)] \equiv \int f(\tau)\exp(-i\Omega\tau)d\tau = \tilde{F}(\Omega)$. The first term in Eq. (A1) is obtained by

$$\int |A_2(t)|^2 F_1(t)\mathcal{T}_F[F_3^*(t,\tau)\exp(i2\omega_1\tau)]dt = \int\int\int dtdt_1d\tau F_1(t)|A_2(t)|^2\exp(-i\Omega t)R^{(\mathrm{TPE})*}(t-t_1)$$
$$\times\exp\{[i\Omega(t-t_1)]\}A_1^*(t_1-\tau)^2\exp\{i(\Omega-2\omega_1)(t_1-\tau)\}$$
$$= \tilde{R}^{(\mathrm{TPE})*}(\Omega)\tilde{A}_{11}^{(2)*}(\Omega-2\omega_1)\int \tilde{A}_{22}^{(2\#)}(\Omega_1)\tilde{F}_1(\Omega-\Omega_1)d\Omega_1$$
$$= \tilde{R}^{(\mathrm{TPE})*}(\Omega)\tilde{A}_{11}^{(2)*}(\Omega-2\omega_1)\int \tilde{A}_{22}^{(2\#)}(\Omega-\Omega_1)\tilde{F}_1(\Omega_1)d\Omega_1$$
$$= \tilde{R}^{(\mathrm{TPE})*}(\Omega)\tilde{A}_{11}^{(2)*}(\Omega-2\omega_1)\int \tilde{A}_{22}^{(2\#)}(\Omega-\Omega_1)\tilde{R}^{(\mathrm{TPE})}(\Omega_1)\tilde{A}_{11}^{(2)}(\Omega_1-2\omega_1)d\Omega_1, \quad \text{(A2)}$$

where $\tilde{F}_1(\Omega)$ is expressed by $\tilde{F}_1(\Omega)=R^{(\mathrm{TPE})}(\Omega)A_1^{(2)}(\Omega-2\omega_1)$. The second term in Eq. (A1) is expressed by

$$\int F_1(t)\mathcal{T}_F[|A_2(t-\tau)|^2F_3^*(t,\tau)\exp(i2\omega_1\tau)]dt = \int\int\int\int d\Omega_1 dtdt_1d\tau F_1(t)\exp(-i\Omega t)A_{22}^{(2\#)}(\Omega_1)R^{(\mathrm{TPE})*}(t-t_1)$$
$$\times\exp\{[i(\Omega+\Omega_1)(t-t_1)]\}A_1^*(t_1-\tau)^2\exp\{i(\Omega+\Omega_1-2\omega_1)(t_1-\tau)\}$$
$$= \tilde{F}_1(\Omega)\int d\Omega_1\tilde{A}_{22}^{(2\#)}(\Omega_1)\tilde{R}^{(\mathrm{TPE})*}(\Omega+\Omega_1)\tilde{A}_{11}^{(2)*}(\Omega+\Omega_1-2\omega_1)$$
$$= \tilde{R}^{(\mathrm{TPE})}(\Omega)\tilde{A}_{11}^{(2)}(\Omega-2\omega_1)\int d\Omega_1\tilde{A}_{22}^{(2\#)}(\Omega_1-\Omega)\tilde{R}^{(\mathrm{TPE})*}(\Omega_1)\tilde{A}_{11}^{(2)*}(\Omega_1-2\omega_1)$$
$$= \tilde{R}^{(\mathrm{TPE})}(\Omega)\tilde{A}_{11}^{(2)}(\Omega-2\omega_1)\left[\int \tilde{A}_{22}^{(2\#)}(\Omega-\Omega_1)\tilde{R}^{(\mathrm{TPE})}(\Omega_1)\tilde{A}_{11}^{(2)}(\Omega_1-2\omega_p)d\Omega_1\right]^*, \quad \text{(A3)}$$

where we used $\tilde{A}_{22}^{(2\#)*}(\Omega-\Omega_1)=\tilde{A}_{22}^{(2\#)}(\Omega_1-\Omega)$. We can obtain Eq. (26) from Eqs. (A2) and (A3).

2. Derivation of the FWM-IAC signal under Raman resonance

We calculate the FW-IAC signal under the Raman resonance. From Eq. (29), the absolute square of the nonlinear polarization in FWM under the Raman resonance is obtained by

$$|P^{(\mathrm{Raman})}(t,\tau)|^2 = |E_1(t,\tau)|^2\left|\int dt_1R^{(\mathrm{Raman})}(t-t_1)E_1(t_1,\tau)E_2^*(t_1,\tau)^2\right|$$
$$= C_1(t,\tau)+C_2(t,\tau)\exp(i\omega_2\tau)+C_2^*(t,\tau)\exp(-i\omega_2\tau)+C_3(t,\tau)\exp(i\omega_1\tau)+C_3^*(t,\tau)\exp(-i\omega_1\tau)+C_4(t,\tau)$$
$$\times\exp\{i(\omega_1+\omega_2)\tau\}+C_4^*(t,\tau)\exp\{-i(\omega_1+\omega_2)\tau\}+C_5(t,\tau)\exp\{i(\omega_1-\omega_2)\tau\}+C_5^*(t,\tau)\exp\{-i(\omega_1-\omega_2)\tau\}$$
$$+C_6(t,\tau)\exp(i2\omega_1\tau)+C_6^*(t,\tau)\exp(-i2\omega_1\tau)+C_7(t,\tau)\exp\{i(2\omega_1-\omega_2)\tau\}+C_7^*(t,\tau)\exp\{-i(2\omega_1-\omega_2)\tau\}$$
$$+C_8(t,\tau)\exp\{i(2\omega_1+\omega_2)\tau\}+C_8^*(t,\tau)\exp\{-i(2\omega_1+\omega_2)\tau\}, \quad \text{(A4)}$$

where we define $C_1(t,\tau)$, $C_2(t,\tau)$, $C_3(t,\tau)$, $C_4(t,\tau)$, $C_5(t,\tau)$, $C_6(t,\tau)$, $C_7(t,\tau)$, and $C_8(t,\tau)$ as

$$C_1(t,\tau) = \{[|A_1(t)|^2+|A_1(t-\tau)|^2][|G_1(t)|^2+|G_2(t,\tau)|^2+|G_3(t,\tau)|^2+|G_4(t,\tau)|^2]+A_1^*(t)A_1(t-\tau)$$
$$\times[G_1(t)G_3^*(t,\tau)+G_2^*(t,\tau)G_4(t,\tau)]+A_1(t)A_1^*(t-\tau)[G_1^*(t)G_3(t,\tau)+G_2(t,\tau)G_4^*(t,\tau)]\},$$

$$C_2(t,\tau) = \{[|A_1(t)|^2+|A_1(t-\tau)|^2][G_1^*(t)G_4(t,\tau)+G_2(t,\tau)G_3^*(t,\tau)]+A_1(t)A_1^*(t-\tau)G_1^*(t)G_2(t,\tau)+A_1^*(t)A_1(t-\tau)G_3^*(t,\tau)G_4(t,\tau)\},$$

$$C_3(t,\tau) = \{[|A_1(t)t|^2+|A_1(t-\tau)|^2][G_1(t)G_3^*(t,\tau)+G_2^*(t,\tau)G_4(t,\tau)]$$
$$\times+A_1(t)A_1^*(t-\tau)[|G_1(t)|^2+t|G_2(t,\tau)|^2+|G_3(t,\tau)|^2+|G_4(t,\tau)|^2]\},$$

$$C_4(t,\tau) = \{[|A_1(t)|^2+|A_1(t-\tau)|^2]G_3^*(t,\tau)G_4(t,\tau)+A_1(t)A_1^*(t-\tau)[G_1^*(t)G_4(t,\tau)+G_2(t,\tau)G_3^*(t,\tau)]\},$$

$$C_5(t,\tau) = \{[|A_1(t)|^2+|A_1(t-\tau)|^2]G_1(t)G_2^*(t,\tau)+A_1(t)A_1^*(t-\tau)[G_1(t)G_4^*(t,\tau)+G_2^*(t,\tau)G_3(t,\tau)]\},$$

$$C_6(t,\tau) = A_1(t)A_1^*(t-\tau)[G_1(t)G_3^*(t,\tau) + G_2^*(t,\tau)G_4(t,\tau)],$$

$$C_7(t,\tau) = A_1(t)A_1^*(t-\tau)G_1(t)G_2^*(t,\tau),$$

$$C_8(t,\tau) = A_1(t)A_1^*(t-\tau)G_3^*(t,\tau)G_4(t,\tau). \tag{A5}$$

We take the derivative of Eq. (35). The Fourier transform of $C_5(t,\tau)$ is described by

$$\mathcal{T}_F[C_5(t,\tau)] = \int dt|A_1(t)|^2 G_1(t)\mathcal{T}_F[G_2^*(t,\tau)\exp\{i(\omega_1-\omega_2)\tau\}] + \int dt G_1(t)\mathcal{T}_F[|A_1(t-\tau)|^2 G_2^*(t,\tau)\exp\{i(\omega_1-\omega_2)\tau\}]$$
$$+ \int dt A_1(t)G_1(t)\mathcal{T}_F[A_1^*(t-\tau)G_4^*(t,\tau)\exp\{i(\omega_1-\omega_2)\tau\}] + \int dt A_1(t)\mathcal{T}_F[A_1^*(t-\tau)G_2^*(t,\tau)G_3(t,\tau)\exp\{i(\omega_1-\omega_2)\tau\}]. \tag{A6}$$

The first, second, third, and fourth terms in Eq. (A6) are obtained by

$$\int dt|A_1(t)|^2 G_1(t)\mathcal{T}_F[G_2^*(t,\tau)\exp\{i(\omega_1-\omega_2)\tau\}] = \int\int\int dt dt_1 d\tau |A_1(t)|^2 G_1(t)\exp(-i\Omega t)R^{(\mathrm{Raman})*}(t-t_1)$$
$$\times\exp\{i\Omega(t-t_1)\}A_1^*(t_1-\tau)A_2(t_1-\tau)\exp\{i(\Omega-\omega_1+\omega_2)(t_1-\tau)\}$$
$$= \tilde{R}^{(\mathrm{Raman})*}(\Omega)\tilde{A}_{12}^{(2\#)*}(\Omega-\omega_1+\omega_2)\int \tilde{A}_{11}^{(2\#)}(\Omega-\Omega_1)G_1(\Omega_1)d\Omega_1$$
$$= G_1^*(\Omega)\int \tilde{A}_{11}^{(2\#)}(\Omega-\Omega_1)G_1(\Omega_1)d\Omega_1, \tag{A7}$$

$$\int G_1(t)\mathcal{T}_F[|A_1(t-\tau)|^2 G_2^*(t,\tau)\exp\{i(\omega_1-\omega_2)\tau\}]dt = \int\int\int\int d\Omega_1 dt dt_1 d\tau \tilde{A}_{11}^{(2\#)}(\Omega_1)G_1(t)\exp(-i\Omega t)R^{(\mathrm{Raman})*}(t-t_1)\exp\{i(\Omega$$
$$+\Omega_1)(t-t_1)\}A_1^*(t_1-\tau)A_2(t_1-\tau)\exp\{i(\Omega+\Omega_1-\omega_1+\omega_2)(t_1-\tau)\}$$
$$= \tilde{G}_1(\Omega)\int d\Omega_1 \tilde{A}_{11}^{(2\#)}(\Omega_1)\tilde{R}^{(\mathrm{Raman})*}(\Omega+\Omega_1)\tilde{A}_{12}^{(2\#)*}(\Omega+\Omega_1-\omega_1+\omega_2)$$
$$= \tilde{G}_1(\Omega)\left[\int \tilde{A}_{11}^{(2\#)}(\Omega-\Omega_1)\tilde{R}^{(\mathrm{Raman})*}(\Omega_1)\tilde{A}_{12}^{(2\#)}(\Omega_1-\omega_1+\omega_2)d\Omega_1\right]^*$$
$$= \tilde{G}_1(\Omega)\left[\int \tilde{A}_{11}^{(2\#)}(\Omega-\Omega_1)\tilde{G}_1(\Omega_1)d\Omega_1\right]^*, \tag{A8}$$

$$\int dt A_1(t)G_1(t)\mathcal{T}_F[A_1^*(t-\tau)G_4^*(t,\tau)\exp\{i(\omega_1-\omega_2)\tau\}] = \int\int\int\int d\Omega_1 dt_1 dt d\tau \tilde{A}_1^*(\Omega_1)A_1^*(t_1)\exp\{-i(\Omega-\Omega_1)t_1\}R^{(\mathrm{Raman})*}(t-t_1)$$
$$\times A_1(t)G_1(t)\exp\{-i\Omega_1 t\}A_2(t_1-\tau)\exp\{i(\Omega-\Omega_1-\omega_1+\omega_2)(t_1-\tau)\}$$
$$= \int d\Omega_1 \tilde{A}_1^*(\Omega_1)A_1^*(\Omega_1-\Omega)\tilde{R}^{(\mathrm{Raman})*}(\Omega_1)\int \tilde{A}_1(\Omega_2)\tilde{G}_1(\Omega_1-\Omega_2)d\Omega_2\tilde{A}_2(\Omega_1$$
$$-\Omega+\omega_1-\omega_2), \tag{A9}$$

$$\int dt A_1(t)\mathcal{T}_F[A_1^*(t-\tau)G_2^*(t,\tau)G_3(t,\tau)\exp\{i(\omega_1-\omega_2)\tau\}]$$
$$= \int\int\int d\Omega_1 dt d\tau \tilde{A}_1^*(\Omega_1)A_1(t)\exp\{-i\Omega_1 t\}G_2^*(t,\tau)G_3(t,\tau)\exp\{-i(\Omega-\Omega_1-\omega_1+\omega_2)\tau\}$$
$$= \int\int\int d\Omega_1 dt \tilde{A}_1^*(\Omega_1)A_1(t)\exp\{-i\Omega_1 t\}\int d\Omega_2 G_3(t,\Omega_2)G_2^*(t,\Omega_2-\Omega+\Omega_1+\omega_1-\omega_2), \tag{A10}$$

where $\tilde{G}_1(\Omega)$ is given by $\tilde{G}_1(\Omega)=\tilde{R}^{(\mathrm{Raman})}(\Omega)\tilde{A}_{12}^{(2\#)}(\Omega-\omega_1+\omega_2)$. Here, $G_2(t,\Omega)$ and $G_3(t,\Omega)$ are expressed by

$$G_2(t,\Omega) = \iint dt_1 d\tau R^{(\mathrm{Raman})}(t-t_1)\exp\{-i(\omega_1-\omega_2-\Omega)(t-t_1)\}A_1(t_1-\tau)A_2^*(t_1-\tau)\exp\{i\Omega(t_1-\tau)\}\exp\{i(\omega_1-\omega_2-\Omega)t\}$$
$$= \tilde{R}^{(\mathrm{Raman})}(\omega_1-\omega_2-\Omega)\tilde{A}_{12}^{(2\#)}(-\Omega)\exp\{i(\omega_1-\omega_2-\Omega)t\}, \tag{A11}$$

and

$$G_3(t,\Omega) = \iint dt_1 d\tau R^{(\mathrm{Raman})}(t-t_1)A_2^*(t_1)\exp\{i(\omega_1-\omega_2-\Omega)t_1\}A_1(t_1-\tau)\exp\{i\Omega(t_1-\tau)\}$$
$$= \tilde{A}_1(-\Omega)\int dt_1 R^{(\mathrm{Raman})}(t-t_1)A_2^*(t_1)\exp\{i(\omega_1-\omega_2-\Omega)t_1\}, \tag{A12}$$

respectively. Using Eqs. (A11) and (A12), Eq. (A10) is rewritten as

$$\int dt A_1(t)\mathcal{T}_F[A_1^*(t-\tau)G_2^*(t,\tau)G_3(t,\tau)\exp\{i(\omega_1-\omega_2)\tau\}]$$
$$= \int\int\int\int dt_1 dt d\Omega_1 d\Omega_2 \tilde{A}_1^*(\Omega_1)\tilde{A}_1(-\Omega_2)A_2^*(t_1)\exp\{i(\omega_1-\omega_2-\Omega_2)t_1\}A_1(t)R^{(\mathrm{Raman})}(t-t_1)$$
$$\times\exp\{-i(\Omega-\Omega_2)t\}\tilde{R}^{(\mathrm{Raman})*}(\Omega-\Omega_1-\Omega_2)\tilde{A}_{12}^{(2\#)*}(\Omega-\Omega_1-\Omega_2-\omega_1+\omega_2)$$
$$= \iint d\Omega_1 d\Omega_2 \tilde{A}_1^*(\Omega_1)\tilde{A}_1(-\Omega_2)\tilde{A}_2^*(\omega_1-\omega_2-\Omega_2)\tilde{A}_1(\Omega-\Omega_2)\tilde{R}^{(\mathrm{Raman})}(\Omega-\Omega_2)G_1^*(\Omega-\Omega_1-\Omega_2)$$
$$= \int d\Omega_2 \tilde{A}_1(-\Omega_2)\tilde{A}_1(\Omega-\Omega_2)\tilde{R}^{(\mathrm{Raman})}(\Omega-\Omega_2)\tilde{A}_2^*(\omega_1-\omega_2-\Omega_2)\int d\Omega_1 \tilde{A}_1^*(\Omega_1)G_1^*(\Omega-\Omega_1-\Omega_2)$$
$$= \int d\Omega_1 \tilde{A}_1(-\Omega_1)\tilde{A}_1(\Omega-\Omega_1)\tilde{R}^{(\mathrm{Raman})}(\Omega-\Omega_1)\tilde{A}_2^*(\omega_1-\omega_2-\Omega_1)\int d\Omega_2 \tilde{A}_1^*(\Omega_2)G_1^*(\Omega-\Omega_1-\Omega_2)$$
$$= \int d\Omega_1(\Omega_1)\tilde{A}_1(\Omega-\Omega_1)\tilde{A}_1(\Omega_1)\tilde{R}^{(\mathrm{Raman})}\tilde{A}_2^*(\Omega-\Omega_1+\omega_1-\omega_2)\int d\Omega_2 \tilde{A}_1^*(\Omega_2)G_1^*(\Omega_1-\Omega_2). \tag{A13}$$

We can obtain Eq. (35) from Eqs. (A7)–(A9) and Eq. (A13).

[1] W. Denk, J. H. Strickler, and W. W. Webb, Science **248**, 73 (1990).
[2] K. König, J. Microsc. **200**, 83 (2000).
[3] R. Hellwarth and P. Christensen, Opt. Commun. **12**, 318 (1974).
[4] J. N. Gannaway and C. J. R. Sheppard, Opt. Quantum Electron. **10**, 435 (1978).
[5] Y. Barad, H. Eisenberg, M. Horowitz, and Y. Silberberg, Appl. Phys. Lett. **70**, 922 (1997).
[6] M. Müller, J. Squier, K. R. Wilson, and G. J. Brankenhoff, J. Microsc. **191**, 266 (1998).
[7] M. D. Duncan, J. Reintjes, and T. J. Manuccia, Opt. Lett. **7**, 350 (1982).
[8] A. Zumbusch, G. R. Holtom, and X. S. Xie, Phys. Rev. Lett. **82**, 4142 (1999).
[9] K. Isobe, S. Kataoka, R. Murase, W. Watanabe, T. Higashi, S. Kawakami, S. Matsunaga, K. Fukui, and K. Itoh, Opt. Express **14**, 786 (2006).
[10] K. Isobe, Y. Ozeki, T. Kawasumi, S. Kataoka, S. Kajiyama, K. Fukui, and K. Itoh, Opt. Express **14**, 11204 (2006).
[11] C. Xu and W. W. Webb, J. Opt. Soc. Am. B **13**, 481 (1996).
[12] L. J. Richter, T. P. Petralli-Mallow, and J. C. Stephenson, Opt. Lett. **23**, 1594 (1998).
[13] J. Tretzel and F. W. Schneider, Chem. Phys. Lett. **59**, 514 (1978).
[14] M. Müller and J. M. Schins, J. Phys. Chem. B **106**, 3715 (2002).
[15] H. Kano and H. Hamaguchi, Appl. Phys. Lett. **86**, 121113 (2005).
[16] P. M. Felker and G. V. Hartland, Chem. Phys. Lett. **134**, 503 (1987).
[17] G. V. Hartland and P. M. Felker, J. Phys. Chem. **91**, 5527 (1987).
[18] M. Bellini, A. Bartoli, and T. W. Hansch, Opt. Lett. **22**, 540 (1997).
[19] J. A. McGuire, W. Beck, X. Wei, and Y. R. Shen, Opt. Lett. **24**, 1877 (1999).
[20] J. A. McGuire and Y. R. Shen, J. Opt. Soc. Am. B **23**, 363 (2006).
[21] J. P. Ogilvie, Kevin J. Kubarych, A. Alexandrou, and M. Joffre, Opt. Lett. **30**, 911 (2005).

[22] J. P. Ogilvie, E. Beaurepaire, A. Alexandrou, and M. Joffre, Opt. Lett. **31**, 480 (2006).
[23] J. Jasapara and W. Rudolph, Opt. Lett. **24**, 777 (1999).
[24] Y. Ozeki, G. Omura, and K. Itoh, Opt. Express **16**, 2778 (2008).
[25] T. Brabec and F. Krausz, Phys. Rev. Lett. **78**, 3282 (1997).
[26] J. Cheng, A. Volkmer, L. D. Book, and X. S. Xie, J. Phys. Chem. B **105**, 1277 (2001).
[27] G. Patterson, R. N. Day, and D. Piston, J. Cell Sci. **114**, 837 (2001).